External beam irradiation angle measurement using Cerenkov emission I: Signal dependencies consideration.

Emilie Jean[1,2,3], Simon Lambert-Girard[4], François Therriault-Proulx[4] and Luc Beaulieu[1,2]

[1] Département de physique, de génie physique et d'optique et Centre de recherche sur le cancer, Université Laval, Quebec, QC, Canada
[2] Département de radio-oncologie et Axe Oncologie du CRCHU de Québec, CHU de Québec - Université Laval, Quebec, QC, Canada
[3] Département de radio-oncologie du CIUSSS-MCQ, CHAUR de Trois-Rivières, Trois-Rivières, QC, Canada
[4] Medscint inc. Quebec, QC, Canada
E-mail: Luc.Beaulieu@phy.ulaval.ca

Received xxxxxx
Accepted for publication xxxxxx
Published xxxxxx

Abstract

This study introduces a novel hybrid Cerenkov-scintillation dosimeter which is intended to be used for irradiation angle measurements based on the Cerenkov angular dependency. First measurements aimed at validating the ability to account for the Cerenkov electron energy spectrum dependency by simultaneously measuring the deposited dose, thus isolating signal variations resulting from the angular dependency. The Cerenkov probe is composed of a 10-mm long sensitive volume of clear PMMA optical fiber separated by an absorptive filter from a 1-mm diameter transport fiber. Both filtered and raw Cerenkov signals from the sensitive volume and transport fiber, respectively, were collected using the Hyperscint RP-200 (Medscint, Quebec) scintillation dosimetry platform. The total signal was unmixed using a hyperspectral approach to eliminate the transport fiber signal contribution. Dose calibration of the detector signal was accomplished with photon (6 and 18 MV) and electron (6-20 MeV) beams. Using a solid-water phantom, measurements at fixed incident angles covering a wide range of doses and output factors were realized. For fixed incident angle, signal characterization of the Cerenkov detector displays a linear dose-light relationship for the whole range of doses tested with various beam energies. As expected, the sensitive volume signal was found to be energy dependent. Output factors were accurately measured within ±0.8 % for field size up to 25x25 cm^2 with both photons and electrons. First validation of the Cerenkov angular dependency shows a linear dose-light relationship for the whole range of angles tested. As expected, the Cerenkov signal intensity per dose unit varies based on the irradiation angle due to the angular dependency. Results showed that using calibration conditions where the electron energy spectrum is similar to the measurement conditions allows to rely on deposited dose to account for this dependency. These preliminary results constitute a first step toward experimental irradiation angle measurements.

Keywords: Cerenkov radiation, scintillation dosimetry, hybrid detector

1. Introduction

In the context of radiotherapy treatments, interest for Cerenkov emission dosimetry has increased over the past decades. While most emerging techniques are focusing on in-vivo Cerenkov imaging (Tendler *et al* 2020, Hachadorian *et al* 2020) or in-water detection with an out-of-field detector (Glaser *et al* 2013, 2014, Pogue *et al* 2015, Meng *et al* 2019, Zlateva *et al* 2019a, 2019b, Yogo *et al* 2020), few are based on Cerenkov light produced in optical fibers (Jang *et al* 2013, Yoo *et al* 2013). Challenges of using Cerenkov signal from an optical fiber arise from the delimitation of a sensitive volume and the signal discrimination of the Cerenkov also produced in the transport fiber itself.

Cerenkov emission is generated in all the optical fiber exposed to the beam due to high energy electrons traveling in a medium at speeds greater than the local speed of light, and is then collected by a photodetector (Beddar *et al* 1992, Boer *et al* 1993). The number of Cerenkov photons emitted is directly dependent of the velocity of the electrons travelling through the medium, and hence their energy (Jelley 1958). Thus, there is a proportionality between the intensity of the emitted light and the dose deposited in the irradiated portion of the optical fiber. It is however necessary to determine the intensity of the signal produced in a finite sensitive volume to link it to the deposited dose. Despite this proportionality, the Cerenkov light intensity collected also possesses an angular dependency (Law *et al* 2006, 2007). This results from the optical photons that are emitted in the shape of a cone with the path of the charged particle as its axis. Moreover, the optical fiber properties will also greatly affect the capture and transmission of the emitted signal depending on the angle formed by the radiation source and the fiber axis. Consequently, Cerenkov light has long been considered a contamination signal in plastic scintillating fiber dosimeters and many techniques have been developed over the past years to overcome its influence in the output signal (Frelin *et al* 2005, Archambault *et al* 2006, Lambert *et al* 2008, Liu *et al* 2011). However, it could be of interest to take advantage of this angular dependency not for dosimetry but rather for irradiation angle measurements.

In this study, we introduce a novel hybrid Cerenkov-scintillation dosimeter that exploits Cerenkov light generated in clear PMMA optical fiber. The detector is designed to simultaneously performed dose measurements and identify the primary photon or electron beam incident angles based on Cerenkov angular dependency. The present paper aims at evaluating the ability to isolate Cerenkov signal variations arising from angular dependency by accounting for other dependencies. A first-built prototype is characterized using 6 and 18 MV photon and 6 to 20 MeV electron beams to validate the Cerenkov dose-light relationship for fixed irradiation angles in various measurements conditions. An extended characterization of the angular dependency and real-time applications of the detector based on this approach for dose and incident angle measurements using various modalities are presented in a companion paper (Jean *et al* 2021a).

2. Materials and methods

2.1 Cerenkov radiation

Cerenkov radiation is an emission of optical photons that occurs when a charged particle travels through a dielectric medium with a velocity greater than the local velocity of light (Cherenkov 1934, Jelley 1958). The time-dependent dipole moment resulting from the asymmetric alignment of the dipoles formed by the polarized molecules generates spherical electromagnetic waves. As the charged particle moves faster than the speed of light in the medium, the emitted waves add up constructively leading to a coherent radiation. The resulting optical photons are emitted in the shape of a cone with the path of the charged particle as its axis, and having a half-opening angle θ defined by

$$\cos\theta = \frac{1}{\beta n}, \tag{1}$$

where n is the refractive index of the medium and β is the relativistic phase velocity of the particle. The latter is defined as

$$\beta = \sqrt{1 - \left(\frac{m_0 c^2}{E + m_0 c^2}\right)^2}, \tag{2}$$

where E is the energy of the charged particle, m_o is the rest mass of the particle and c the velocity of light in vacuum. The threshold energy E_{th}, that is the minimal energy required to generate Cerenkov radiation, can be defined by rearranging equation (2) using a velocity greater than the local speed of light such as

$$E_{th} = m_0 c^2 \left(\frac{1}{\sqrt{1 - \frac{1}{n^2}}} - 1\right). \tag{3}$$

The Cerenkov yield, that is the number of optical photons dN in the wavelength interval between λ_1 and λ_2 emitted per unit path length dl of a charged particle having an energy greater than E_{th}, is given by the Frank–Tamm formula (Tamm and Frank 1937)

$$\frac{dN}{dl} = 2\pi\alpha z^2 \left(1 - \frac{1}{\beta^2 n^2}\right)\left(\frac{1}{\lambda_2 - \lambda_1}\right), \tag{4}$$

where α is the dimensionless fine-structure constant and z the charge of the particle.

Considering an optical fiber having a PMMA-based core with refractive index of 1.49 (at 520 nm), the minimal energy required for an electron to generate Cerenkov radiation is 178 keV. Thus, external beams from medical linear accelerator (LINAC) composed of photons or electrons will induce in the exposed optical fiber and surrounding media a polyenergetic

electron fluence spectrum of which most of the electrons possess an energy greater than the threshold (McLaughlin *et al* 2018, Konefał *et al* 2015). According to Equation (4), the number of optical photons emitted within the fiber increases with the particle energy and the refractive index. The same also applies to the cone semi-angle θ calculated using Equation (1). However, influence of the refractive index variation of PMMA over the visible spectrum (i.e., 400-700 nm) is considered negligible (Zhang *et al* 2020). Therefore, Cerenkov light emission intensity and angle mostly depend on the energy fluence spectrum. According to Equation (2), the energy has a greater impact for electrons of approximately 1.0 MeV or less. As the particle energy becomes less relativistic and approaches the threshold energy, the phase velocity β decreases significantly, resulting in an angular dependency shifting toward lower angles.

2.2 Cerenkov transmission in multimode fiber

Once generated, only a small fraction of the Cerenkov light produced in the core is captured and transmitted along the transport fiber. The total intensity reaching the photodetector depends on the angle between the fiber axis and the particle path. It is also strongly affected by the transport fiber physical properties and total length. Law *et al.* (Law *et al* 2006) studied the capture of the Cerenkov light and its transmission along a multimode transport fiber. It was shown that the range of angles over which Cerenkov light is propagated and the maximum intensity angle depend on the core–cladding refractive index difference Δn ($n_{core} - n_{clad}$). A greater Δn increases the fiber numerical aperture and allows more of the Cerenkov cone to be captured. Moreover, as the numerical aperture increases, the peak intensity angle shifts toward lower angles. Considering the energy dependency of the Cerenkov yield and angle, the capture and transmission are also affected by the depth of measurement. As electron energy loss increases with the travelled distance, the slowing-down process induces fewer Cerenkov photons with lower angle between the fiber axis and the particle path due to the narrowing of the cone opening. Measurements performed in the penumbra region would also affect the Cerenkov yield due to the lack of primary particles. Consequently, the angular dependency of the Cerenkov light is linked to the optical fiber type and measurement conditions.

2.3 Detector conception

Using the Cerenkov radiation induced in optical fiber implies the delimitation of a sensitive volume to discriminate the signal also produced in the transport fiber itself. Delimiting a finite volume also allows to link the signal to the deposited dose. While the Cerenkov signal is not directly dose dependent, there is a proportionality between the two of them as both directly depend on the electron energy spectrum. To rely on this proportionality, a precise measurement of the dose deposition in the sensitive volume must also be performed simultaneously. Thus, the hybrid Cerenkov-scintillation dosimeter designed for this study was composed of two distinct probes as shown in Figure 1. A first fiber-based Cerenkov detector was built similarly as a single-point plastic scintillation dosimeter (PSD). A 10 mm long optical fiber with a PMMA-based core and fluorinated polymer-based cladding (1 mm diameter ESKA GH-4001, Mitsubitshi Chemical Co., Tokyo, Japan) was used as a finite sensitive volume. The latter was separated by an absorptive filter from a 17 m long transport fiber (ESKA GH-4001) to modify the Cerenkov spectrum produced in the sensitive volume, thus allowing for an algorithm to properly eliminate the contamination signal from the transport fiber. An absorptive filter was preferred to guarantee no light emission was reflected towards its emission source. To increase the total signal collected, the same type of fiber was used to generate and conduct the Cerenkov light to a photodetector due to its high core-cladding refractive index difference Δn of 0.11. All components were bonded together using an optical adhesive and sealed with a 3D printed (SL1 printer, Prusa, Prague, Czech Republic) light tight tube made of photo-hardening polyresin.

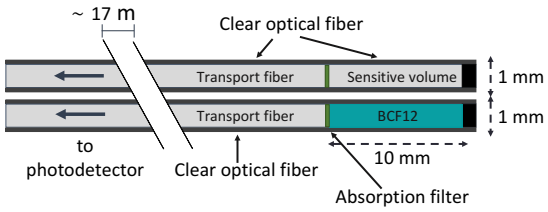

Figure 1 : Design schematic of the hybrid detector showing the Cerenkov and the scintillation probe assemblies.

An independent similarly built PSD composed of a 10 mm long BCF12 scintillating fiber (Saint-Gobain, Hiram, USA) was also used for simultaneous dose measurements. As the Cerenkov detector signal intensity depends on both irradiation angle and electron energy spectrum, the scintillating probe provides a real-time dose measurement. Normalizing the Cerenkov probe signal to the deposited dose should allow to eliminate the electron energy spectrum dependency. The remaining Cerenkov signal variations are then linked to the angular distribution of primary and scattered electrons having an energy greater than the threshold E_{th}. Consequently, signal variations attributable to angular dependency could be used to extract the irradiation angle with an angular calibration curve performed under fixed dose irradiations.

2.4 Signal acquisition set-up

Irradiations of the detector were performed using a Varian Clinac IX (Varian Medical Systems, Palo Alto, USA) linear accelerator with the detector placed along the lateral axis. The

multi-channel HYPERSCINT scintillation dosimetry platform (HYPERSCINT RP-200, Medscint Inc., Quebec, Canada) was used to collect simultaneously the light signal emitted by both probes of the detector (Jean *et al* 2021b). The transport fibers of 17 m long allowed to place the HYPERSCINT platform outside the treatment room to minimize noise and prevent any damage to the electronic components of the photodetector. All measurements were performed using a wavelength range set from 350 to 635 nm which represents an effective area of 2260 pixels wide on the photodetector. To reduce the readout noise, a binning was performed in the vertical direction of the sensor on 100 pixels for each channel and the cooling system was set at -5˚ C to keep the temperature stable across all measurements. Each acquisition was made using a repetitive 2 s integration time. The probes being light shielded, no precaution needs to be taken to prevent ambient light contamination. Nevertheless, background exposures with matching exposure time were taken and subtracted from the acquired signal.

2.5 Signal unmixing

As both probes of the detector possess their own light guide, their respective signal was collected and unmixed independently using the hyperspectral approach (Archambault *et al* 2012). The measured spectrum (m) is assumed to be a linear superposition of the normalized spectra (r_i) of the different light emitting sources such as

$$m = \sum_{i=1}^{n} r_i x_i, \tag{5}$$

where x_i represents the contribution of each light emission sources i. As the BCF12 and the clear fiber probes are constructed as single-point PSD, only the scintillation and the filtered Cerenkov from the sensitive volume contributes to the measurement, respectively. The total measured spectrum also includes two contamination signals from the transport fiber that is exposed to the beam, which are unfiltered Cerenkov and fluorescence (Nowotny 2007, Boer *et al* 1993, Therriault-Proulx *et al* 2013). Thus, the variable n in this study is equal to 3 to account for all light emission sources.

As the sensor array used for spectrum measurements is *2260* pixels wide, each of them is considered as L individual measurement channels to which are assigned a wavelength (λ_j). This can be expressed in matrix form such as

$$\begin{bmatrix} m_{\lambda 1} \\ m_{\lambda 2} \\ \vdots \\ m_{\lambda L} \end{bmatrix} = \begin{bmatrix} r_{1,\lambda 1} & r_{2,\lambda 1} & \dots & r_{n,\lambda 1} \\ r_{1,\lambda 2} & r_{2,\lambda 2} & \cdots & r_{n,\lambda 2} \\ \vdots & \vdots & \vdots & \vdots \\ r_{1,\lambda L} & r_{2,\lambda L} & \cdots & r_{n,\lambda L} \end{bmatrix} \begin{bmatrix} x_1 \\ x_2 \\ \vdots \\ x_n \end{bmatrix}. \tag{6}$$

To solve this system for the variable x, the left pseudo-inverse matrix method is used as follows

$$x = (R^T R)^{-1} R^T m. \tag{7}$$

The raw spectrum of each element that contributes to the total signal measured is required to solve Equation (7). Contrary to plastic scintillator detectors, it is not possible to use a beam with lower energy than the Cerenkov threshold to obtain raw spectra of the Cerenkov probe sensitive volume in absence of the transport fiber contamination signal. Accordingly, a procedure similar to the one described by Guillot et al. (Guillot *et al* 2011) was used. As illustrated in Figure 2, the probe was irradiated in 3 respective conditions. C2 and C3 measurements are performed using an irradiation angle where the fluorescence to Cerenkov ratio is minimized (i.e. at the maximal Cerenkov emission angle) while the C1 measurement is performed at normal incidence using a known dose validated with a Farmer ionization chamber (TN 31013, PTW, Freiburg, Germany). The difference between calibration measurements C3 and C2 is only due to contamination signal as the dose received to the sensitive volume in both conditions is identical. Therefore, the contamination signal is then used to unmix the C1 measurement signal and hence extract the sensitive volume raw spectrum. As for the fluorescence, 60 cm of rolled transport fiber was directly placed on the exit window of the On-Board Imaging kV source arm (OBI, Varian Medical Systems, Palo Alto, USA). The latter was set at 120 kVp for a 20 seconds irradiation which is under the Cerenkov production energy threshold in PMMA. Thus, for irradiation conditions where the fluorescence to Cerenkov ratio is greater than the calibration conditions, additional fluorescence contribution can be considered by the linear unmixing algorithm.

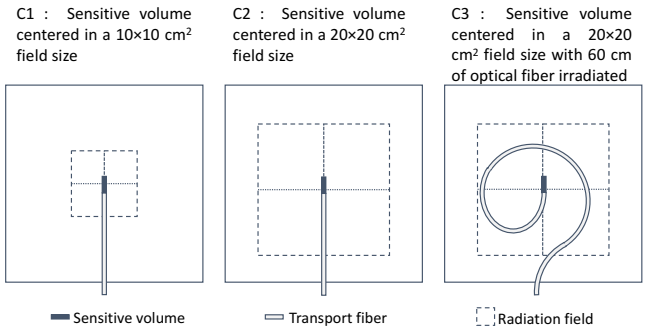

Figure 2 : Schematic showing the three different configurations used for the calibration measurements.

2.6 Dose calibration

The dose calibration of the detector signal is obtained using Eq (7). The intensity ($x_{i,C1}$) calculated for the deposited dose ($d_{i,C1}$) with irradiation C1 is then used to determine the dose received in other irradiation conditions (d_i) such as

$$d_i = d_{i,C1}\frac{x_i}{x_{i,C1}}. \quad (8)$$

While the equation (8) is valid for any irradiation conditions when using a scintillation detector, nominal energy, angle and depth of measurement must match those of the calibration irradiation for a Cerenkov detector. Otherwise, correction factors should be used to account for intensity variation that arise from other dependencies when the detector is used for dosimetry purpose. Consequently, the Cerenkov detector signal was dose calibrated at a d_{max} depth (i.e. 1.5 cm at 6 MV, 3.5 cm at 18 MV, 1.5 cm at 6 MeV, 2 cm at 9 MeV and 3 cm at 12, 16 and 20 MeV) and at normal incidence for this study.

3. Prototype validation

3.1 Dose linearity

First measurements aimed at evaluating the efficiency of the absorptive filter to produce a sufficiently distinct Cerenkov spectrum allowing for the linear unmixing algorithm to properly eliminate the contamination signal from the transport fiber. Given that, the Cerenkov probe was used in the same manner as a PSD. That is, the sensitive volume signal was characterized as a function of the deposited dose. Dose linearity measurements were performed using the clear fiber probe signal as a function of the deposited dose measured by the scintillator. Both were embedded in a solid water phantom at a d_{max} depth, and a 10 cm thick slab was placed underneath to provide backscatter. Using 6 and 18 MV photon and 6 to 20 MeV electron beams, the sensitive volume and the scintillator were positioned at the isocentre. Irradiations with doses ranging from 20 cGy to 500 cGy in a 10x10 cm^2 field size were performed at normal incidence with respect to the fiber axis (i.e., Gantry at 0˚ with the probes along the lateral axis).

3.2 Output factors

Output factor measurements were realized at normal incidence for field sizes varying from 5×5 to 25×25 cm^2 using 3 repeated irradiations of 100 cGy at 6 and 18 MV and 6, 9, 12, 16 and 20 MeV, respectively. The detector was embedded in a solid water phantom at a d_{max} depth with sufficient backscatter material. The sensitive volumes of the two probes were centered at the treatment isocentre. In order to calculate the relative outputs, the signal measured with both probes at field size $n \times n$ cm^2, using jaw-defines fields for photons and applicator size for electrons, was normalized to the signal measured under a 10×10 cm^2 field. All relative output factors were validated using a TN 31013 ionization chamber (PTW, Freiburg, Germany) using the same set-up and acquisition routine.

3.3 Dose rate independence

Validation of the dose rate independence was achieved at normal incidence using the same solid water phantom with both probes placed at a d_{max} depth at the centre of a 10x10 cm^2 field size at normal incidence. The surface-to-source distance (SSD) was gradually increased to reduce the mean dose rate. For each couch position, respectively five irradiations of 200 cGy at 600 MU/min were realized under 6 and 18 MV photon beams. To account for the field size variation, attenuation in air, and treatment room backscattering at high SDD, absolute dose rate measurements relative to SSD were performed with a TN 31013 ionization chamber. The Cerenkov probe measured doses were then normalized to the ionization chamber values.

3.4 Angular dependency

A first validation of the angular dependency was obtained with both probes inserted in a water-equivalent cylindrical 3D printed (MK3S+ printer, Prusa, Prague, Czech Republic) phantom to ensure a constant depth of measurement regardless of the gantry angle. The solid cylinder of 6 cm diameter composed of a methacrylate polymers resin (Polyresin-Tough, Prusa Polymers, Prague, Czech Republic) was used to perform irradiations of the detector at 6 and 18 MV but also 12, 16 and 20 MeV. For the 6 and 9 MeV beams, a smaller cylinder of 3 cm diameter was also built (SL1 printer, Prusa, Prague, Czech Republic). Due to the reduced electron range, this ensured a sufficient signal would be produced. Both probes were placed along the lateral axis with their sensitive volumes centered at the isocentre and pointing toward the X2 jaw. To avoid any attenuation of the beam from the treatment table, the phantom was suspended in the air at the foremost longitudinal position as illustrated in Figure 3. Irradiations ranging from 20 cGy to 500 cGy using a 10×10 cm^2 field size were repeated at various Gantry angles between 0˚ to 90˚.

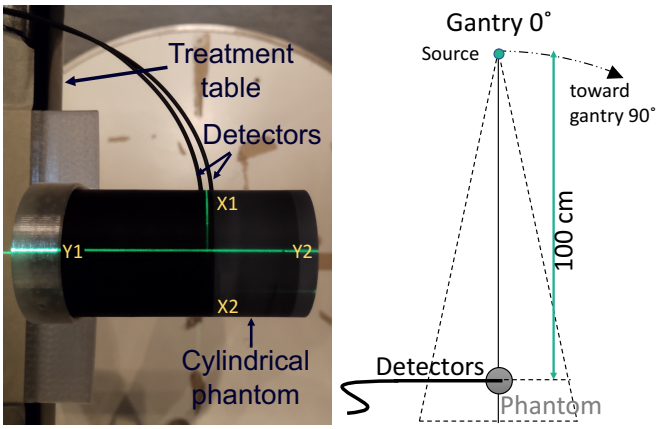

Figure 3 : (Left) Top view of the set-up used for the validation of the Cerenkov prototype showing the 2 probes inserted in the 3D printed cylindrical phantom placed on its stand. (Right) Schematic of the phantom showing the orientation of the probes with respect to the Gantry position.

4. Results

4.1 Signal unmixing

The three spectra composing the signal measured by the Cerenkov probe, including the filtered Cerenkov from the sensitive volume as well as the two contamination signals, are shown in Figure 4.a. The signature shape of the sensitive volume spectrum results from the notch absorptive filter that was chosen to build the prototype. All spectra were normalized to their respective maxima for the purpose of the linear unmixing process.

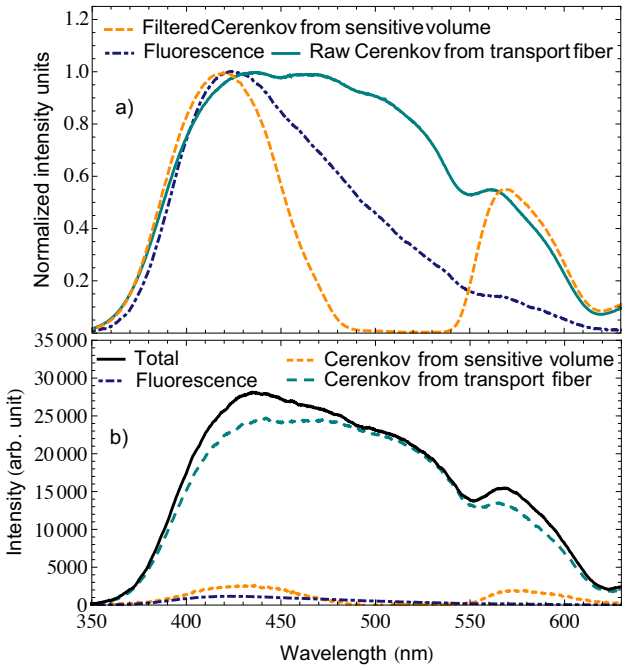

Figure 4 : (a) Normalized spectra of each light emitting component of the Cerenkov probe used to perform the signal unmixing . (b) Total intensity measured for a 100 cGy irradiation and individual spectra of each light emitting element of the Cerenkov detector. All spectra are affected by the wavelength response of the photodetection system and the transport fiber transmission spectrum.

An example of the Cerenkov probe total intensity measured under a 100 cGy irradiation at normal incidence and the different light emitting source contributions are illustrated in Figure 4.b. A portion of the total measured spectrum includes some intensity due to fluorescence produced in the transport fiber as the fluorescence to Cerenkov ratio was greater than the calibration measurement conditions. The contribution of the 1 cm long sensitive volume represents only a slight fraction of the total intensity collected as the probe was irradiated with a field size of 10 x 10 cm^2.

4.2 Dose linearity

Results obtained for the signal characterization of the Cerenkov probe under 6 and 18 MV photon beams at normal incidence for various doses are shown in Figure 5.a. Results for the same measurements using 6 to 20 MeV electron beams are presented in Figure 5.b. The signal intensity of the Cerenkov sensitive volume was found to follow a linear trend as a function of the dose measured with the scintillation signal for both modalities used. The influence of the energy on the measured intensity was found to vary according to the radiation beam type. While the intensity collected for a given dose tends to increase with energy for the photon beams, an opposite tendency was observed for the electrons. As the Frank-Tamm formula predicts a greater yield with increasing energy, this observation is only valid at normal incidence and the trend at the peak intensity angle should obey the predicted energy dependency. Nevertheless, various angular measurements must be performed to characterize this dependency.

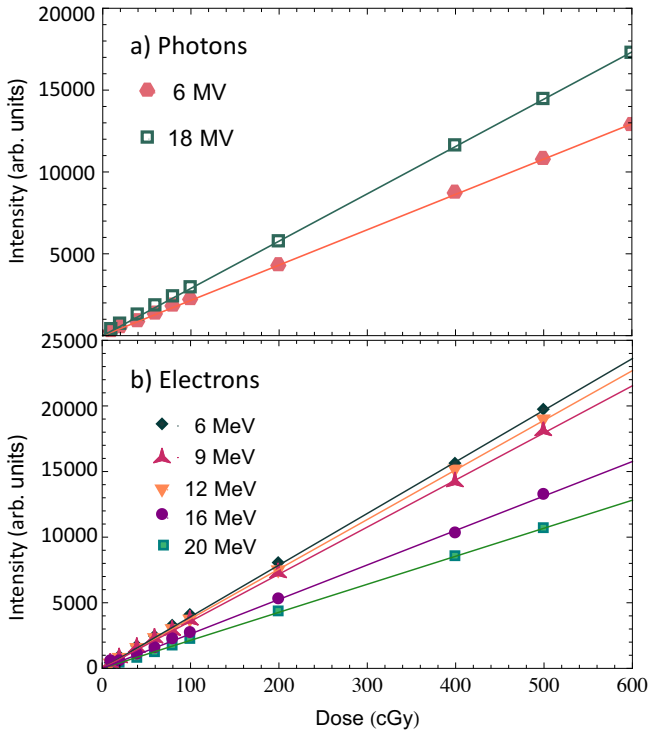

Figure 5 : Signal emitted by the Cerenkov detector sensitive volume as a function of the dose obtained with (a) 6 and 18 MV photon beams and (b) 6, 9, 12, 16 and 20 MeV electron beams at normal incidence. All coefficients of determination are above 0.99991.

4.3 Output factors

Table 1 displays relative output factors obtained with the Cerenkov and the scintillation probes under 6 and 18 MV photon beams. Compared to ionization chamber measurements, relative output factors were accurately measured within ±0.8 % using the Cerenkov probe at 6 and 18 MV. As shown in Table 2, the primary particle type did not affect the dose measurements as the Cerenkov detector provided similar accuracy with various electron energies.

Table 1 : Photon beam relative output factors normalized to a 10 x 10 cm^2 field size measured with the Cerenkov and scintillation detector in comparison with a TN30013 Farmer ionization chamber (PTW, Freiburg, Germany) and their relative differences.

Energy	*Field size (cm^2)*	*Ionization chamber*	*Cerenkov detector*	*Relative difference (%)*	*BCF12 detector*	*Relative difference (%)*
6 MV	5 x 5	0.942	0.950	0.8	0.944	0.2
	10 x10	1	1	-	1	-
	15 x15	1.032	1.031	-0.1	1.031	-0.1
	20 x 20	1.053	1.047	-0.6	1.055	0.2
	25 x 25	1.067	1.066	-0.1	1.076	0.8
18 MV	5 x 5	0.901	0.908	0.8	0.909	0.9
	10 x10	1	1	-	1	-
	15 x15	1.045	1.049	0.5	1.044	-0.1
	20 x 20	1.071	1.071	-0.03	1.065	-0.6
	25 x 25	1.086	1.083	-0.3	1.084	-0.2

Table 2 : Electron beam relative output factors normalized to a 10 x 10 cm^2 field size measured with the Cerenkov and scintillation detector in comparison with a TN30013 Farmer ionization chamber (PTW, Freiburg, Germany) and their relative differences.

Energy	*Applicator size (cm^2)*	*Ionization chamber*	*Cerenkov detector*	*Relative difference (%)*	*BCF12 detector*	*Relative difference (%)*
6 MeV	6 x 6	0.964	0.964	0	0.966	0.3
	10 x10	1	1	-	1	-
	15 x15	1.005	1.007	0.2	1.008	0.3
	20 x 20	1.012	1.010	-0.2	1.010	-0.2
	25 x 25	1.006	1.007	-0.2	1.014	0.8
9 MeV	6 x 6	0.975	0.977	0.8	0.980	0.5
	10 x10	1	1	-	1	-
	15 x15	0.994	0.993	0.3	0.991	-0.3
	20 x 20	0.983	0.975	-0.8	0.980	-0.3
	25 x 25	0.962	0.968	0.6	0.960	-0.2
12 MeV	6 x 6	0.963	0.956	-0.7	0.966	0.3
	10 x10	1	1	-	1	-
	15 x15	0.989	0.989	0	0.989	0
	20 x 20	0.976	0.982	0.6	0.975	-0.1
	25 x 25	0.949	0.942	-0.7	0.947	-0.2
16 MeV	6 x 6	0.987	0.984	-0.3	0.993	0.6
	10 x10	1	1	-	1	-
	15 x15	0.982	0.984	0.2	0.983	0.1
	20 x 20	0.966	0.965	-0.1	0.969	0.3
	25 x 25	0.937	0.940	0.3	0.938	0.1
20 MeV	6 x 6	1.006	1.004	-0.2	1.009	0.3
	10 x10	1	1	-	1	-
	15 x15	0.973	0.966	-0.6	0.971	-0.2
	20 x 20	0.950	0.951	0.1	0.950	0
	25 x 25	0.922	0.926	0.4	0.918	-0.4

While the transport fiber length exposed to the beam increases with the field size and consequently reduces the ratio of the sensitive volume signal to contamination signal, it did not impinge the precision. The average accuracy of the Cerenkov detector is similar to what was observed with the BCF12 detector.

4.4 Dose rate independence

At normal incidence, the measured dose using the Cerenkov sensitive volume signal was found to be dose-rate independent, as expected.

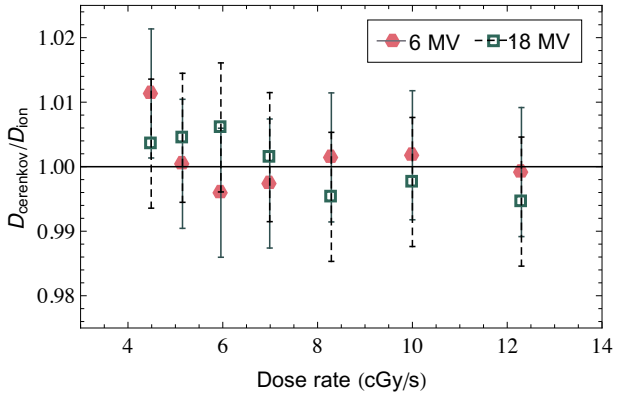

Figure 6 : Measured dose at normal incidence with the Cerenkov detector normalized to an ionization chamber as a function of the dose rate.

Figure 6 depicts the dose ratio of the Cerenkov detector to the ionization chamber as a function of the mean dose rate. For fixed dose irradiations, the sensitive volume signal shows a discrepancy with the predicted dose that reaches 1.1 % at 6 MV for the lowest dose rate tested. Similar results were obtained under an 18 MV photon beam and the dose was accurately measured within ±0.7 %.

4.5 Angular dependency

The signal intensity of the Cerenkov probe as a function of the dose measured with the scintillation probe at various angles are presented in Figure 7.a and Figure 7.b for 6 and 18 MV photon beams, respectively. While the linear dose-light relationship can be observed for the whole range of angles tested at both energies, the slope of the regression varies based on the irradiation angle due to the Cerenkov angular dependency. Same results were also obtained with the electron beams (not shown). For all Gantry angles and energies tested, the lowest regression slope coefficient of determination was found to be 0.99991.

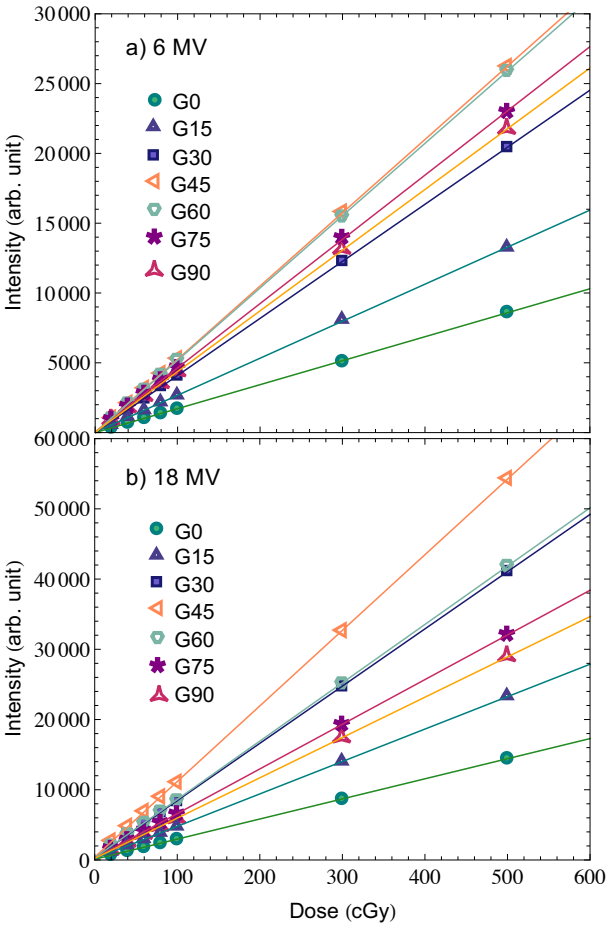

Figure 7 : Signal emitted by the Cerenkov detector sensitive volume as a function of the dose obtained with (a) 6 MV and (b) 18 MV photon beams at various Gantry angles ranging from 0° to 90°.

The signal intensities of the Cerenkov probe per unit of dose measured with the scintillation probe as a function of the irradiation angle are presented in Figure 8.a and 8.b for photon and electron beams, respectively. Comparing the results at various energies shows that the angular dependency also varies as a function of the beam energy. For the photon beams, the intensity per dose unit increases as a function of the energy for all angles. For the electron beams, the intensity collected at normal incidence for a given dose tends to decrease with energy as illustrated in Figure 8.b. However, the trend at the peak intensity angle obeys the predicted dependency with a greater yield for increasing energy.

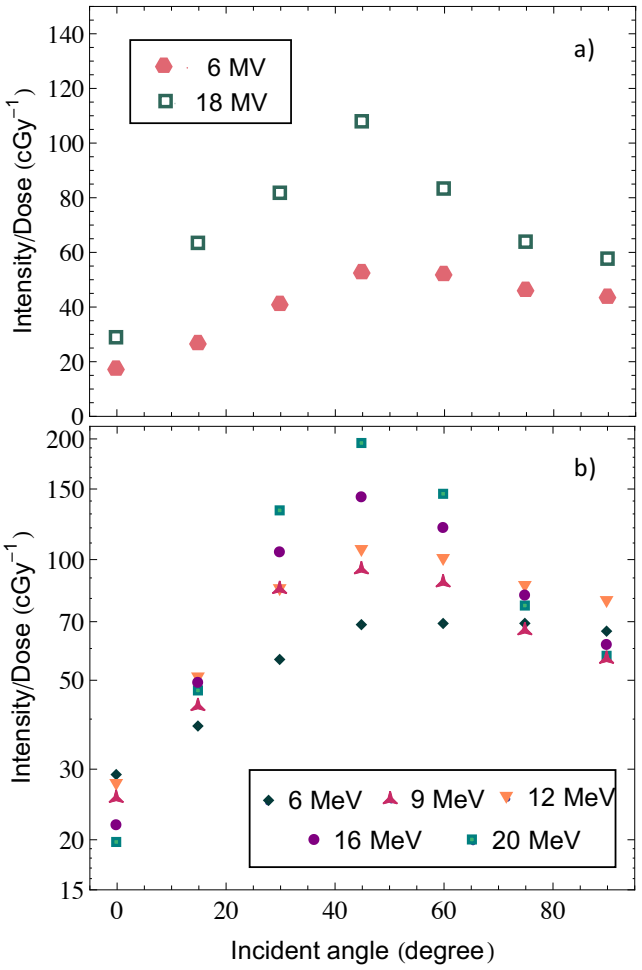

Figure 8 : Ratios of the signal emitted by the Cerenkov detector sensitive volume to the deposited dose as a function of the irradiation angle obtained with (a) 6 and 18 MV photon and (b) 6, 9, 12, 16 and 20 MeV electron beams.

5. Discussion

5.1 Cerenkov probe dose-light relationship

Characterization of the relationship between the Cerenkov probe sensitive volume signal collected and the deposited dose is of great interest to validate the suitability of the detector. As the Cerenkov probe was used in the same manner as a PSD for this study, it allowed to validate the proportionality of the Cerenkov signal and the dose for all modalities and energies tested. While there is no direct dependency between the two of them, they both share an electron energy spectrum dependency. Consequently, results showed that using calibration conditions where the electron energy spectrum is identical to the measurement conditions allows to rely on deposited dose to account for this dependence.

5.2 Contamination signal influence

We investigated the accuracy of output factor measurements using the Cerenkov probe and did a comparison with the scintillator for a wide range of field sizes. The reason for this test was to compare the efficiency of the Cerenkov signal separation method as the contamination signal increases. While the algorithm worked properly for a constant contamination to sensitive volume signal ratio, it was necessary to validate that an increase of the contamination signal resulting from larger field sizes would not affect the Cerenkov probe accuracy. It was found that both detectors provide similar accuracy for all field sizes and modalities tested. This result is a pre-requisite as the dose measured by the scintillation detector is intended to eliminate the electron energy spectrum dependency of the Cerenkov signal. Furthermore, the dose rate independence measurements were also conducted with increasing field size as a function of the SSD. While the dose was accurately measured within ±0.8% with the Cerenkov probe at 18 MV, a greater difference was observed with the 6 MV beam at the lowest dose rate. This discrepancy arises from the total signal that decreases as the electron fluence is reduced for larger SSD.

5.3 Energy and angular dependency

The nominal energy of the beam has shown to influence the total intensity collected as a function of dose. In agreement with the Frank-Tamm formula, the 18 MV beam induced a greater amount of Cerenkov light in the sensitive volume than at 6 MV. At the peak intensity, that is approximately twice the number of optical photons for a given dose that are collected using the 18 MV beam. Moreover, the intensity per Gy as a function of the irradiation angle was also found to vary according to energy. The most significant differences between the 6 and 18 MV beam measurements can be observed for gantry angles ranging between 45˚ and 90˚ (Figure 8). While a greater variation of intensity per dose unit as a function of the irradiation angle can be observed at 18 MV for this interval, the regression slope values obtained at 6 MV only showed minor changes. This results from the increase of electrons having lower energy which consequently shifts the angular dependency toward lower angles between the fiber axis and the particle paths. Thus, it allows more of the Cerenkov cone to be captured. The difference between the angular dependency of the two energies also arises from the particle paths. In fact, the secondary electrons resulting from Compton effect at higher energies tends to be scattered forward (Andreo *et al* 2017). Accordingly, the Cerenkov angular dependency at 18 MV will be exacerbated as the particle paths better reflects the irradiation angle.

As for the electron beams, measurements performed at normal incidence shows that the intensity collected per dose unit declines as a function of the energy. This is counter-intuitive as the Cerenkov yield is supposed to increase with energy according to Frank-Tamm formula. This irregularity at

normal incidence is also attributable to the electron paths that tend to go forward at higher energies. Contrarily, lower energy beam provides numerous electrons with arbitrary trajectories that are not related anymore to the beam incident angle. Thus, the Cerenkov angular distribution is broader, and it increases the amount of light reaching the detector at lower angles. Inversely, the signal at higher energies decreases due to the narrowing of the Cerenkov cone. At the peak intensity angle, the 20 MeV beam induced a greater amount of Cerenkov light in the sensitive volume in agreement with the predicted Cerenkov yield. Nonetheless, due to the important variations of the intensity per dose unit as a function of the beam energy for both modalities, a calibration must be performed for each of them to enable the use of the detector for dose or angle measurements.

6. Conclusion

The aim of this study was to introduce a novel Cerenkov-scintillation dosimeter. More precisely, the main objective of the present paper was to evaluate the ability to isolate Cerenkov signal variations arising from angular dependency by accounting for other dependencies. Using a first prototype, the Cerenkov dose-light relationship for fixed angle measurements was validated for 6 and 18 MV photon and 6 to 20 MeV electron beams. While the intensity of the Cerenkov probe signal was found to increase with photon energy, an inverse tendency was observed with the electron beams at normal incidence. Nevertheless, the trend at peak intensity angle agreed with the Frank-Tamm formula for all modalities tested. Using the Cerenkov detector, output factors were accurately measured within ±0.8 % for field size up to 25x25 cm^2 for all energies tested with both photons and electrons. The average accuracy is similar to what was observed with the BCF12 detector even if the scintillation signal is up to 20 times greater than the Cerenkov sensitive volume signal for an exact same length. These results demonstrate the efficiency of the absorptive filter to produce a sufficiently distinct Cerenkov spectrum allowing for the linear unmixing algorithm to properly eliminate the contamination signal from the transport fiber.

Characterization of the Cerenkov-scintillation detector has demonstrated that the Cerenkov probe signal is linear with deposited dose and dose rate independent. The detector was also able to measure accurately clinical photon and electron beams deposited dose. Moreover, performing measurements in conditions where the electron energy spectrum is identical to the calibration conditions allows to rely on the measured dose to account for this dependency. Consequently, resulting signal variations are only attributable to the angular dependency. Although the detector has been employed in the same manner as a PSD for dose measurements in this study, a further characterization of the angular dependency will enable irradiation angle measurements.

Acknowledgements

This work was supported by the *Natural Sciences and Engineering Research Council of Canada* (NSERC) Discovery grants RGPIN 05038-2019 and the Fellowships Program of the *Ministère de la Santé et des Services Sociaux du Québec* (MSSS). François Therriault-Proulx and Simon Lambert-Girard are Co-founder at Medscint inc., a company developing scintillation dosimetry systems. This work was not financially supported by Medscint. The authors thank Benjamin Côté for his help manufacturing the probes and Frédérik Berthiaume for providing technical support with the Hyperscint dosimetry platform.

References

Andreo P, Burns D T, Nahum A E and Seuntjens J 2017 *Fundamentals of Ionizing Radiation Dosimetry: Solutions to the Exercises* (Weinheim: John Wiley & Sons)

Archambault L, Beddar A S, Gingras L, Roy R and Beaulieu L 2006 Measurement accuracy and cerenkov removal for high performance, high spatial resolution scintillation dosimetry *Med Phys* **33** 128–35

Archambault L, Therriault-Proulx F, Beddar S and Beaulieu L 2012 A mathematical formalism for hyperspectral, multipoint plastic scintillation detectors *Phys. Med. Biol.* **57** 7133–45

Beddar A S, Mackie T R and Attix F H 1992 Cerenkov light generated in optical fibres and other light pipes irradiated by electron beams *Phys. Med. Biol.* **37** 925–35

Boer S F de, Beddar A S and Rawlinson J A 1993 Optical filtering and spectral measurements of radiation-induced light in plastic scintillation dosimetry *Phys. Med. Biol.* **38** 945–58

Cherenkov P A 1934 Visible Emission of Clean Liquids by Action of γ Radiation *Dokl. Akad. Nauk SSSR* **2** 451

Frelin A M, Fontbonne J M, Ban G, Colin J, Labalme M, Batalla A, Isambert A, Vela A and Leroux T 2005 Spectral discrimination of Cerenkov radiation in scintillating dosimeters *Med Phys* **32** 3000–6

Glaser A K, Davis S C, Voigt W H A, Zhang R, Pogue B W and Gladstone D J 2013 Projection imaging of photon beams using Čerenkov-excited fluorescence *Phys Med Biol* **58** 601–19

Glaser A K, Zhang R, Gladstone D J and Pogue B W 2014 Optical dosimetry of radiotherapy beams using Cherenkov radiation: the relationship between light emission and dose *Phys. Med. Biol.* **59** 3789–811

Guillot M, Gingras L, Archambault L, Beddar S and Beaulieu L 2011 Spectral method for the correction of the Cerenkov light effect in plastic scintillation detectors: A comparison study of calibration procedures and validation in Cerenkov light-dominated situations *Med Phys* **38** 2140–50

Hachadorian R L, Bruza P, Jermyn M, Gladstone D J, Pogue B W and Jarvis L A 2020 Imaging radiation dose in breast radiotherapy by X-ray CT calibration of Cherenkov light *Nature Communications* **11** 2298

Jang K W, Yagi T, Pyeon C H, Yoo W J, Shin S H, Jeong C, Min B J, Shin D, Misawa T and Lee B 2013 Application of Cerenkov radiation generated in plastic optical fibers for therapeutic photon beam dosimetry *JBO* **18** 027001

Jean E, Girard-Lambert S, Therriault-Proulx F and Beaulieu L 2021a External beam irradiation angle measurement using Cerenkov emission II: Detector characterization and applications

Jean E, Therriault-Proulx F and Beaulieu L 2021b Comparative optic and dosimetric characterization of the HYPERSCINT scintillation dosimetry research platform for multipoint applications *Phys. Med. Biol.* **66** 085009

Jelley J V 1958 *Cerenkov Radiation And Its Applications* (Norwich: Pergamon Press)

Konefał A, Bakoniak M, Orlef A, Maniakowski Z and Szewczuk M 2015 Energy spectra in water for the 6 MV X-ray therapeutic beam generated by Clinac-2300 linac *Radiation Measurements* **72** 12–22

Lambert J, Yin Y, McKenzie D R, Law S and Suchowerska N 2008 Cerenkov-free scintillation dosimetry in external beam radiotherapy with an air core light guide *Phys. Med. Biol.* **53** 3071–80

Law S H, Fleming S C, Suchowerska N and McKenzie D R 2006 Optical fiber design and the trapping of Cerenkov radiation *Appl Opt* **45** 9151–9

Law S H, Suchowerska N, McKenzie D R, Fleming S C and Lin T 2007 Transmission of Čerenkov radiation in optical fibers *Opt. Lett., OL* **32** 1205–7

Liu P Z Y, Suchowerska N, Lambert J, Abolfathi P and McKenzie D R 2011 Plastic scintillation dosimetry: comparison of three solutions for the Cerenkov challenge *Phys. Med. Biol.* **56** 5805–21

McLaughlin D J, Hogstrom K R, Neck D W and Gibbons J P 2018 Comparison of measured electron energy spectra for six matched, radiotherapy accelerators *Journal of Applied Clinical Medical Physics* **19** 183–92

Meng X, Du Y, Wang R, Li Z, Zhu S, Wu H, Li C, Chen W, Nie S, Ren Q and Lu Y 2019 Cherenkov excited luminescence imaging induced by megavolt X-ray beams in the second near-infrared window *Optics Communications* **452** 417–21

Nowotny R 2007 Radioluminescence of some optical fibres *Phys. Med. Biol.* **52** N67–73

Pogue B W, Glaser A K, Zhang R and Gladstone D J 2015 Cherenkov radiation dosimetry in water tanks – video rate imaging, tomography and IMRT & VMAT plan verification *Journal of Physics: Conference Series* **573** 012013

Tamm I E and Frank I M 1937 Coherent radiation of afast electron in a medium *Dokl. Akad. Nauk SSSR* **14** 107–12

Tendler I I, Hartford A, Jermyn M, LaRochelle E, Cao X, Borza V, Alexander D, Bruza P, Hoopes J, Moodie K, Marr B P, Williams B B, Pogue B W, Gladstone D J and Jarvis L A 2020 Experimentally Observed Cherenkov Light Generation in the Eye During Radiation Therapy *International Journal of Radiation Oncology*Biology*Physics* **106** 422–9

Therriault-Proulx F, Beaulieu L, Archambault L and Beddar S 2013 On the nature of the light produced within PMMA optical light guides in scintillation fiber-optic dosimetry *Phys Med Biol* **58** 2073–84

Yogo K, Matsushita A, Tatsuno Y, Shimo T, Hirota S, Nozawa M, Ozawa S, Ishiyama H, Yasuda H, Nagata Y and Hayakawa K 2020 Imaging Cherenkov emission for quality assurance of high-dose-rate brachytherapy *Scientific Reports* **10** 3572

Yoo W J, Shin S H, Jeon D, Hong S, Kim S G, Sim H I, Jang K W, Cho S and Lee B 2013 Simultaneous measurements of pure scintillation and Cerenkov signals in an integrated fiber-optic dosimeter for electron beam therapy dosimetry *Opt. Express, OE* **21** 27770–9

Zhang X, Qiu J, Li X, Zhao J and Liu L 2020 Complex refractive indices measurements of polymers in visible and near-infrared bands *Appl. Opt., AO* **59** 2337–44

Zlateva Y, Muir B R, El Naqa I and Seuntjens J P 2019a Cherenkov emission-based external radiotherapy dosimetry: I. Formalism and feasibility *Med Phys* **46** 2370–82

Zlateva Y, Muir B R, Seuntjens J P and El Naqa I 2019b Cherenkov emission-based external radiotherapy dosimetry: II. Electron beam quality specification and uncertainties *Med Phys* **46** 2383–93